Electronic Supplementary Information

Hollow carbon-shell/carbon-nanorods arrays for high performance Li-ion batteries and supercapacitors

Shengbin Wang, Yalan Xing, Changlei Xiao, Xin Wei, Huaizhe Xu and Shichao Zhang*

Experimental

Synthesis

The peanut-like MnO@C templates were prepared via a carbohydrate coating and graphitization process: 1.4 g of $KMnO_4$ was dissolved into 70 mL of deionized water with magnetic stirring, and then 3 mL of HCl (37 wt%) was added to the solution. The solution was transferred into a Teflon-lined stainless steel autoclave, heated at 140 °C for 12 h. The resulting product was separated, washed and dried to obtain the α-MnO_2 nanotubes hollow sphere. Then, 0.5 g of as-prepared α-MnO_2, 5 g of glucose and 2 g of urea were dispersed into 70 mL of deionized water. The solution was placed into autoclave and heated at 120 °C for 5 h to harvest peanut-like α-MnO_2@organic precursor. Finally, the peanut-like MnO@C was obtained by heating sample at 700 °C for 2 h with the heating-rate of 3°C min^{-1}.

To achieve the N-HPC, 0.5 g MnO@C templates were immersed into 10 mL HCl (37 wt%) at room temperature for 8 h to remove the MnO.

Structural Characterization

Powder X-ray diffraction (XRD) data were collected on a Rigaku D/Max-2400 diffractometer with Cu Kα radiation. Scanning electron microscopy (SEM, Hitachi S-4800), transmission electron microscopy (TEM, JEM-2100F) and high-resolution TEM (HR-TEM, FEI, Tecnai G2 F20) were used to investigate the morphnology and microstructure of the produce. The Brunauer-Emmett-Teller (BET) specific surface area was determined by nitrogen adsorption-desorption at 77 K using a Quantachrome

Autosorb-1C-VP Analyzer. The carbon and nitrogen contents were measured by Vario EL cube organic element analyzer. The Raman spectra was achieved on a labRAM ARAMIS laser Raman spectroscopy under a backscattering geometry. X-ray photoelectron spectra (XPS) were recorded on a Thermo VG ESCALAB250 X-ray photoelectron spectrometer.

Electrochemical Characterization

For the battery test, the working electrode was fabricated by 80% N-HPCs, 10% carbon black and 10% PVDF binder on copper-foil collector with active material loading of around 1.5 mg cm^{-2}. The obtained electrode, polyethene separator and Li metal foil were assembled into a 2032 type coin cell filled with electrolytes (1 M LiPF6 in ethylene carbonate-dimethyl carbonate) in Ar filled glove box. Cyclic voltammograms (CVs) were recorded on CHI 660D electrochemistry workstation at a scan rate of 0.1 mV s^{-1} between 0.01 and 3.0 V *vs.* Li^+/Li. Electrochemical data were collected using NWEARE BTS-610 test system within the potential range of 0.01–3.0 V *vs*. Li^+/Li at various current densities.

For supercapacitors test, the working electrode was fabricated by 80% N-HPCs, 10% carbon black and 10% PVDF binder on anikel foam. The loading mass of active materials was about 5 mg cm^{-2}. All the electrochemical measurements were used 3-electrode system with a voltage range of -1.0-0 (*vs.* Hg/HgO), the sample was used as the test electrode, platinum foil as the counter electrode, Hg/HgO electrode as reference electrode, and 1.0M KOH aqueous solution as electrolyte. CV curves were obtained by varying the scan rate from 5 to 100 m Vs^{-1}. Electrochemical impedance spectroscopy (EIS) was measured in the frequency range of 10 mHz to 10 kHz. Charge-discharge measurements were carried out galvanostatically at 0.5-15.0 A g^{-1}. The specific capacitances in the present case were calculated from galvanostatic charge/discharge curves according to the following equation: $C = \frac{I \times \Delta t}{m \times \Delta V}$

where C (F g^{-1}) is the specific capacitance, I (A) refers to the discharge current, ΔV (V) represents the potential change within the discharge time Δt (s), and m (g) corresponds to the amount of active material on the electrode.

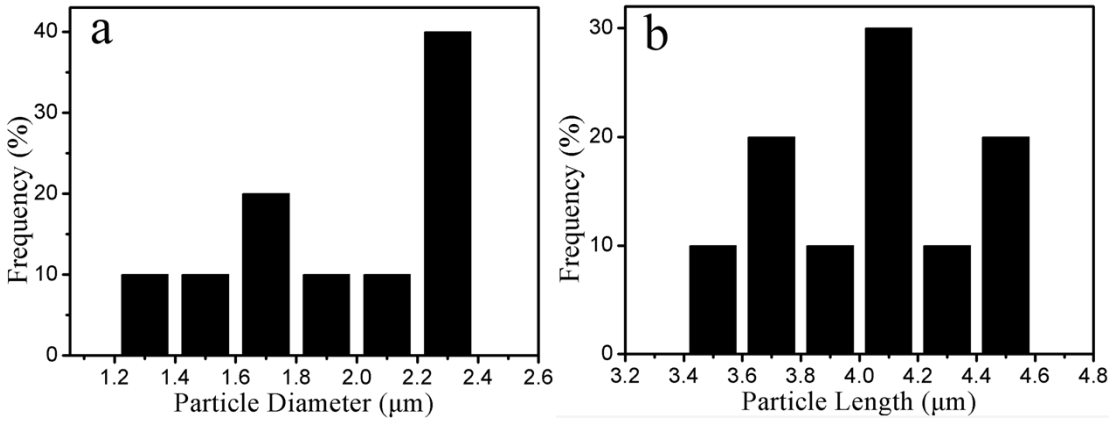

Fig. S1. a) Histogram of the diameter, and b) the length distribution of the N-HPC.

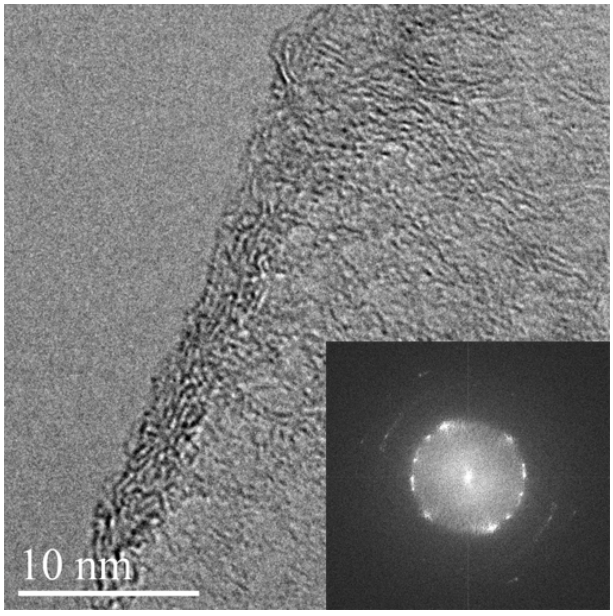

Fig. S2. HRTEM image of the N-HPC, the inset shows the SAD image.

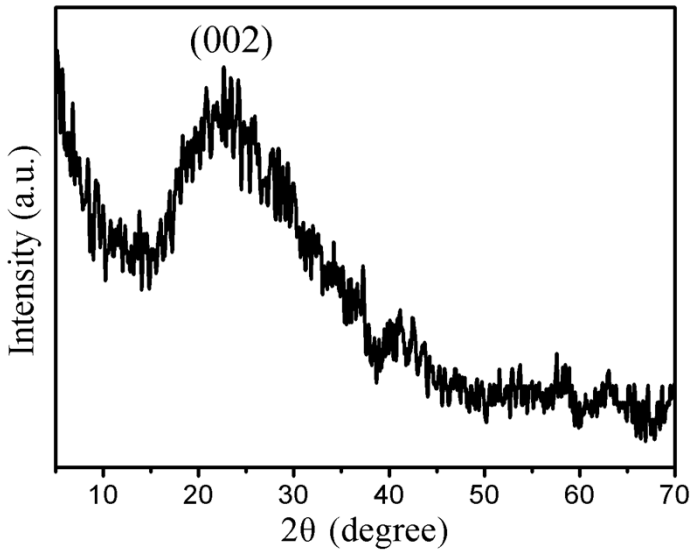

Fig. S3. XRD pattern of the N-HPC.

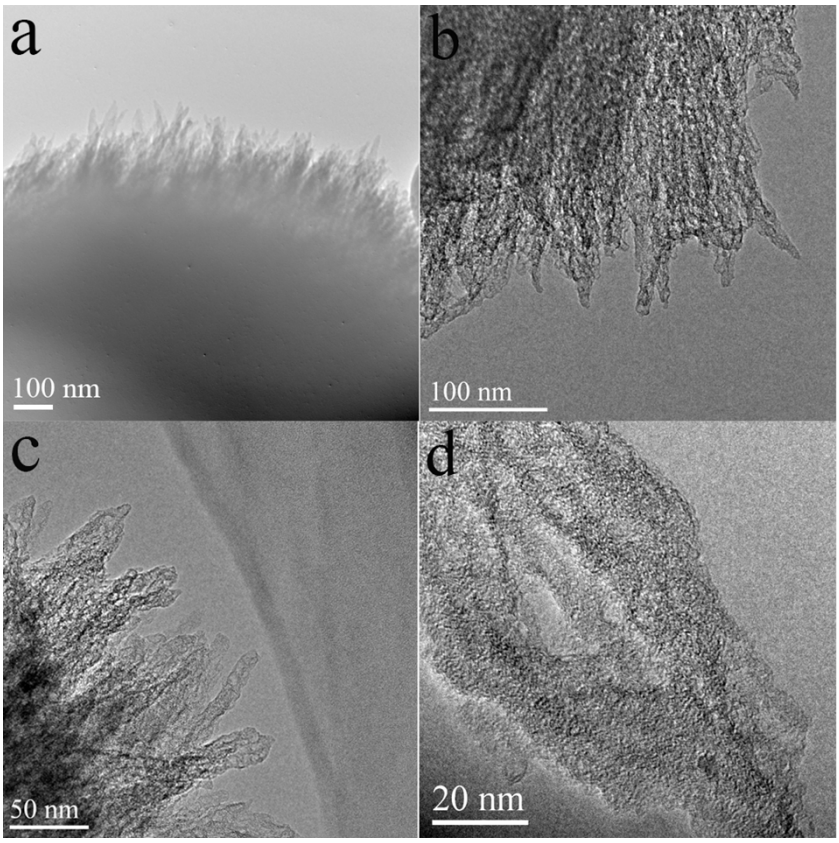

Fig. S4. a) TEM image, b, c, d) and HRTEM images of the N-HPC.

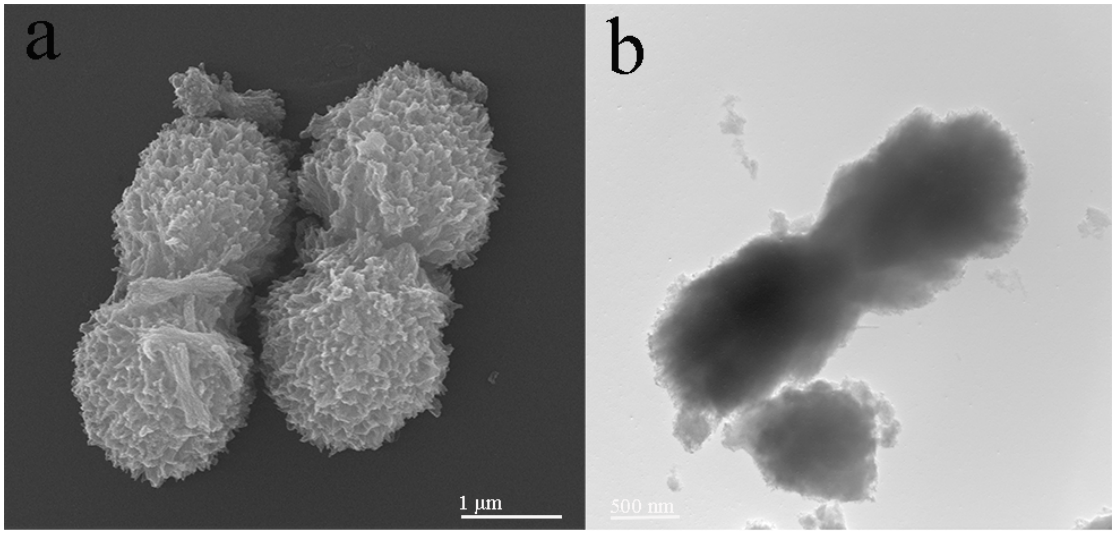

Fig. S5. a) SEM image and b) TEM image of the MnO@C templates.

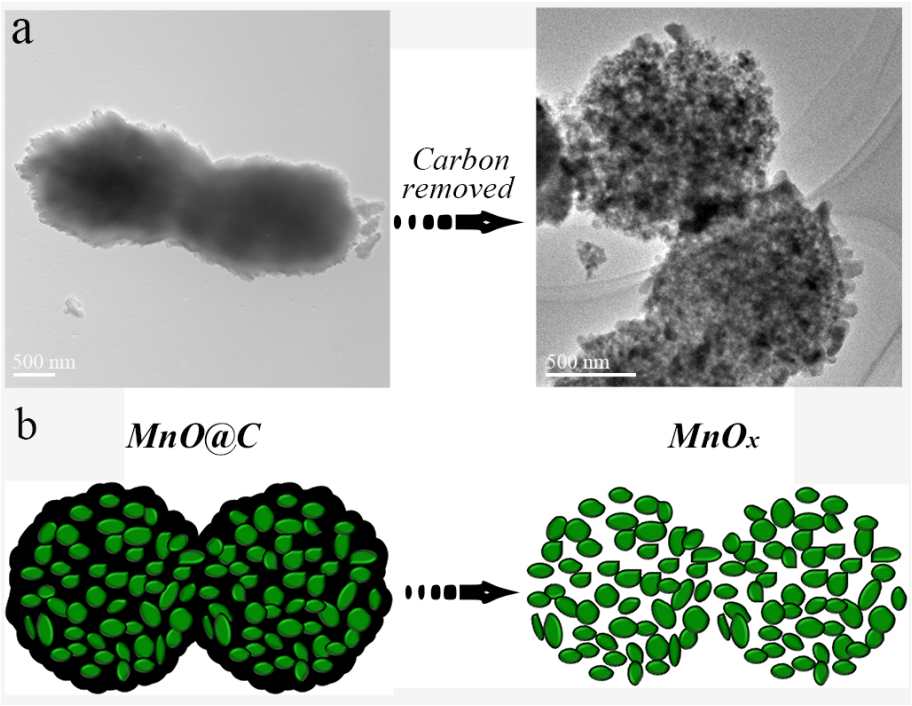

Fig. S6. a) TEM images and b) schematic representation of MnO@C phase structure before and after carbon removal.

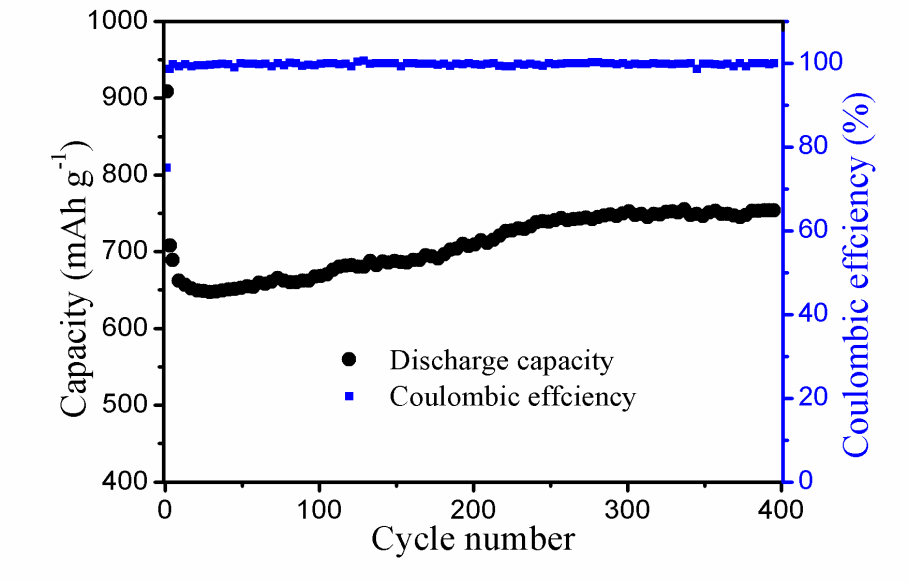

Fig. S7. Cycling performance of the N-HPC at the rate of 1.5 A g^{-1}.

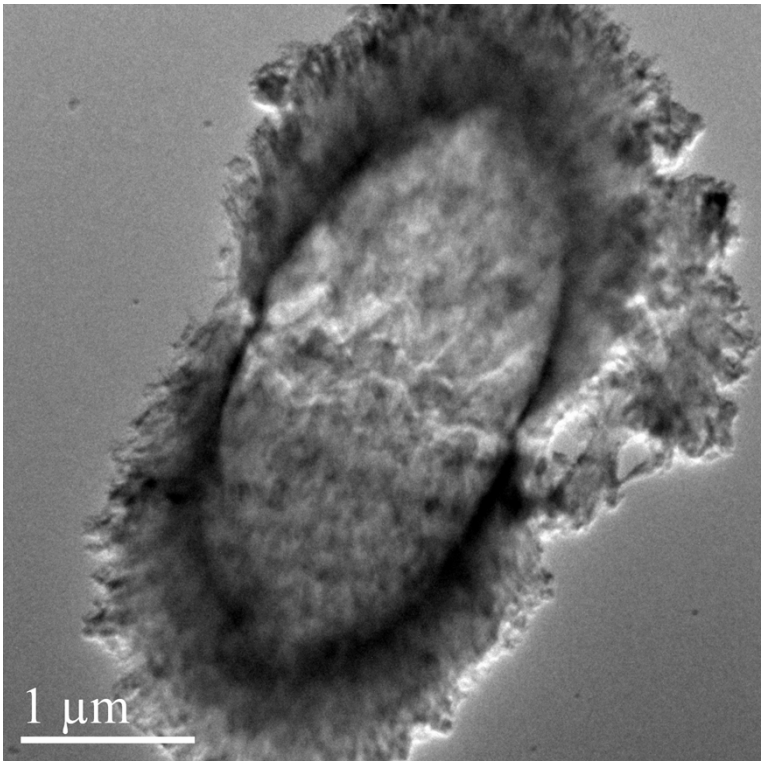

Fig. S8. TEM image of the N-HPC after 200 cycles at the rate of 0.1 A g^{-1}.

Table S1. Comparison of the BET surface area and LIBs performances of N-HPC and some other carbon based materials					
	surface area (m^2 g^{-1})	Reversible capacity (mAh g^{-1})		Rate-retention (%)	Ref.
N-HPC	1322	1003 at 0.1 A g^{-1}	613 at 3 A g^{-1}	61	This work
Hollow Carbon-Nanotube/ Nanofiber	1840	913 at 0.1 A g^{-1}	268 at 3 A g^{-1}	29	S1
Carbon Nanofiber Webs	2381	1280 at 0.1 A g^{-1}	505 at 5 A g^{-1}	39	S2
Hollow carbon cage	1405	1050 at 0.1 A g^{-1}	400 at 2.5 A g^{-1}	38	S3
Porous carbon	916	1129 at 0.185 A g^{-1}	664 at 3.7 A g^{-1}	58	S4
Mesoporous carbon	800	1780 at 0.1 A g^{-1}	205 at 4 A g^{-1}	11	S5
Co_3O_4@graphene	-	941 at 0.2 A g^{-1}	450 at 2 A g^{-1}	47	S6

Table S2. Comparison of the supercapacitor performances of N-HPC and some other carbon based materials				
	electrolyte	Reversible capacity (F g^{-1})		Ref.
N-HPC	1 M KOH	282 at 0.5 A g^{-1}	228 at 15 A g^{-1}	This work
Mesoporous carbon	1 M H_2SO_4	390 at 0.25 A g^{-1}	270 at 10 A g^{-1}	S5
Porous Carbon Nanofibers	6 M KOH	202 at 1 A g^{-1}	164.5 at 30 A g^{-1}	S7
Microporous Carbon	1 M H_2SO_4	340 at 0.1 A g^{-1}	310 at 0.2 A g^{-1}	S8
Carbon–tipped MnO_2/mesoporous carbon/MnO_2	1 M Na_2SO_4	266 at 1 A g^{-1}	170 at 40 A g^{-1}	S9
MnO_2/PEDOT nanowire	1 M Na_2SO_4	210 at 5 mA cm^{-2}	190 at 25 mA cm^{-2}	S10
Carbon nanotube/α-MnOOH coaxial nanocable	1 M Na_2SO_4	202 at 0.65 A g^{-1}	147 at 16.1 A g^{-1}	S11

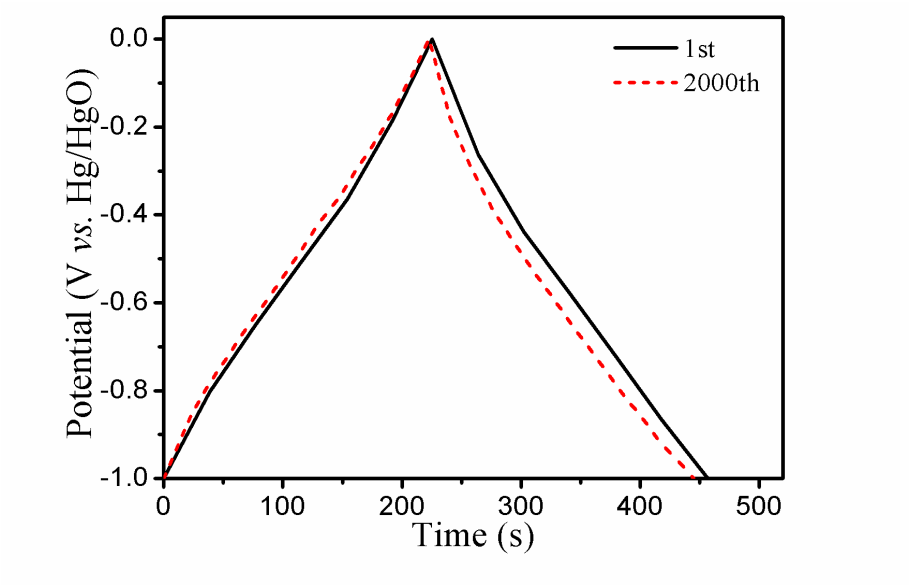

Fig. S9. Triangular shapes of the first and 2000th cycle.

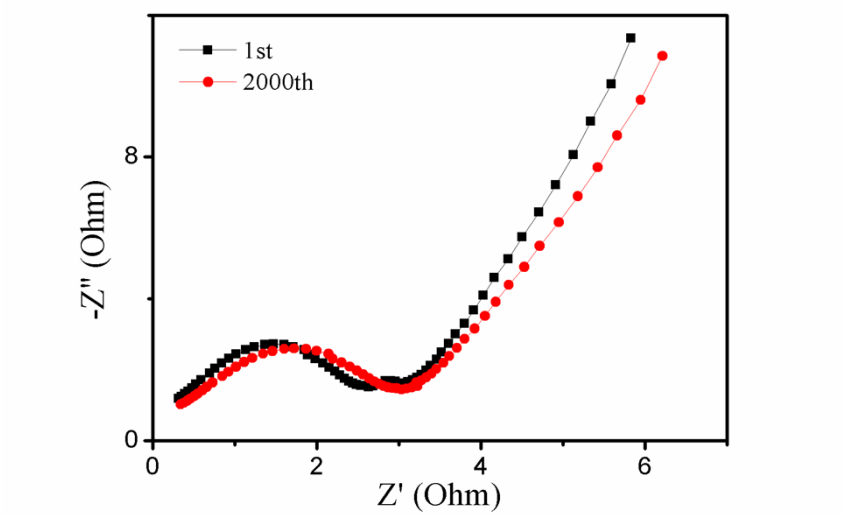

Fig. S10. High frequency EIS of the N-HPC.

References

[S1] Y. Chen, X. Li, K. Park, J. Song, J. Hong, L. Zhou, Y.-W. Mai, H. Huang and J. B. Goodenough, *J. Am. Chem. Soc.*, 2013, **135**, 16280.

[S2] L. Qie, W.-M. Chen, Z.-H. Wang, Q.-G. Shao, X. Li, L.-X. Yuan, X.-L. Hu, W.-X. Zhang, and Y.-H. Huang, *Adv. Mater.,* 2012, **24**, 2047

[S3] G. Zhou, D.-W. Wang, X. Shan, N. Li, F. Li and H.-M. Cheng, *J. Mater. Chem.,* 2012, **22**, 11252.

[S4] L. Chen, Y. Zhang, C. Lin, W. Yang, Y. Meng, Y.Guo, M. Li and D. Xiao, *J. Mater. Chem. A*, 2014, **2**, 9684.

[S5] Z. Li, Z. Xu, X. Tan, H. Wang, C. M. B. Holt, T. Stephenson, B. C. Olsen and David Mitlin, *Energy Environ. Sci.*, 2013, **6**, 871.

[S6] B. Li, H. Cao, J. Shao, G. Li, M. Qu and G. Yin, *Inorg. Chem.,* 2011, **50**, 1628.

[S7] L.-F. Chen, X.-D. Zhang, H.-W. Liang, M. Kong, Q.-F. Guan, P. Chen, Z.-Y. Wu and S.-H. Yu, *ACS Nano,* 2012, **6**, 7092.

[S8] C. O. Ania, V. Khomenko, E. Raymundo-Piñero, J.B. Parra and F. Béguin, *Adv. Funct. Mater.*, 2007, **17**, 1828.

[S9] H. Jiang, L. Yang, C. Li, C. Yan, P. S. Lee and J. Ma, *Energy Environ. Sci.*, 2011, **4**, 1813.

[S10] R. Liu and S. B. Lee, *J. Am. Chem. Soc.*, 2008, **130**, 2942.

[S11] Hua Fang, Shichao Zhang, Xiaomeng Wu, Wenbo Liu, Bohua Wen, Zhijia Du, Tao Jiang, *J. Power Sources,* 2013, **235**, 95.